

Mineral prospectivity mapping: a potential technique for sustainable mineral exploration and mining activities – a case study using the copper deposits of the Tagmout basin, Morocco

Fatima Zahra Echogdali^a, Said Boutaleb^a, El Hassan Abia^a, Mohammed Ouchchen^a, Bouchra Dadi^{a,b}, Mouna Id-Belqas^a, Mohamed Abioui^a, Luan Thanh Pham^c, Tamer Abu-Alam^d and Kevin L. Mickus^e

^aDepartment of Earth Sciences, Faculty of Sciences, Ibn Zohr University, Agadir, Morocco;

^bLaboratory for Sustainable Innovation and Applied Research, Universiapolis - International University of Agadir, Agadir, Morocco; ^cDepartment of Geophysics, Faculty of Physics, University of Science, Vietnam National University, Hanoi, Viet Nam; ^dThe Faculty of Biosciences, Fisheries and Economics, UiT The Arctic University of Norway, Tromsø, Norway; ^eDepartment of Geosciences, Missouri State University, Springfield, Missouri, USA

ABSTRACT

Mineral prospectivity mapping (MPM) based on the principle of geometric mean was applied to stream sediment geochemical, fault density, and aeromagnetic data from Tagmout basin, Morocco to determine new areas for optimizing copper exploration. The application of a fuzzy operator using stream sediment data, factor analysis, and fault density map, allowed weights to be assigned to these parameters so that the MPM function can process them to indicate the most favorable zones of copper mineralization. The model's accuracy as evaluated using a normalized density index (Nd with value 1.22) shows the reliability of the method. The potential copper concentration areas represent 8.22% of the entire basin of which 30% are concentrated in the western portion of the basin and other significant areas are in the southwest and northeast portions. The results indicate that MPM is a powerful technique for planning exploration programs that aim for sustainable mining activities.

Introduction

Prospecting for mineral deposits is a challenging process given that the majority of the large-scale deposits have already been located. The remaining deposits may have smaller geochemical and/or geophysical signatures, be located beneath cover rocks, and/or there is a lack of geological information that makes ore deposits difficult to detect. One technique to overcome these difficulties is to use mineral prospectivity mapping (MPM) to determine regions for more detailed exploration. Mineral prospectivity is a computer-based method that integrates a wide range of geo-information that includes geophysical,

geochemical, geological, and remote sensing (e.g., multispectral satellite data) to determine spatial associations between these data sets with potential ore deposits (Bonham-Carter et al. 1989; Zuo 2020). Several mineral prospectivity methods can be divided into either knowledge-driven or data-driven techniques or combinations between these two end-members (Zuo 2020).

Most mineral prospectivity methods are multi-criteria decision-making (MCDM) routines that are procedures of deciding the best outcome choice from many possible alternatives (Zhang and Liu 2010). In many cases, decision criteria reported by a decision-maker is often inaccurate for several reasons such as the weights are expressed in precise numbers, gaps in data, limited knowledge and insufficient capacity of the decision-maker, or because the decision-maker has an imprecise or inadequate level of information processing in the domain of the problem (Xu and Cai 2010; Wu and Zhang 2011). Accordingly, a fuzzy operator has been used in routines to solve MCDM problems and generate weights for decision criteria (Zadeh 1965; Xu and Cai 2010) and thus, a final decision model. The decision model can then be used to describe the imprecise decision and provide a better way to manage uncertainty in decision making (Wu and Zhang 2011).

In recent years, various methods have been used in MPM, including the data-driven index overlay technique (Yousefi and Carranza 2016), Boolean logic MPM technique (Carranza et al. 2008; Yousefi and Carranza 2016), fuzzy operators (Yousefi and Nykänen 2016), and the expected value MPM method (Yousefi and Carranza 2015a). Yousefi and Carranza (2015b) proposed the geometric average prospectivity model to generate continuously weighted evidential maps. This method provides a number of advantages including a) reduce the uncertainty associated with bias in feature weights and distance intervals to imprecisely estimated features, b) providing fuzzy weights of continuous values into the evidence maps which are assigned without the use of the known mineral occurrences locations, and c) they can also solve the problem of using different values of evidence layers in the same unit (Yousefi and Carranza 2015b).

The evaluation of prospectivity models is a critical problem in defining exploration targets. In this regard, fractal methods (Mandelbrot 1983) can be used with geometric support to estimate the spatial characteristics related to the mineral deposits, such as geochemical anomalies (e.g., Cheng et al. 1994; Cheng 2007; Carranza et al. 2008; Carranza 2010; Afzal et al. 2010, 2016; Zuo 2011a, 2011b; Kouhestani et al. 2020; Pourgholam et al. 2021; Shahbazi et al. 2021; Shamseddin Meigooni et al. 2021), geological structures (e.g., faults) (Carranza and Sadeghi 2010) and geological units (Zuo et al. 2009). Fractal models have been used to classify exploration evidence layers and target areas for prospectivity modeling of minerals (Almasi et al. 2015; Yousefi and Carranza 2015a, 2015b). Many studies have proposed the fractal models using concentration-area (C-A) and prediction-area (P-A) to determine the evidential map capacity with the known mineral occurrences, and determine predictive ability that can be used as an evidential map weight and for selecting thresholds to yield binary predictor maps (e.g., Yousefi et al. 2014; Yousefi and Carranza 2015b, 2016).

This work aims to evaluate the potential of locating additional copper deposits within Tagmout basin in eastern Morocco where several large copper deposits currently exist. Prospectivity models include fractal and geometric averaging methods that will be used to determine higher concentrations of copper occurrences. The models (Figure 1) incorporate geological, geochemical data from stream sediment samples and geophysical (magnetic) data to determine and identify anomalies associated with copper deposits. These anomalies will then be categorized according to their potential as targets for prospecting geology and geophysics in more detail for copper mineralization.

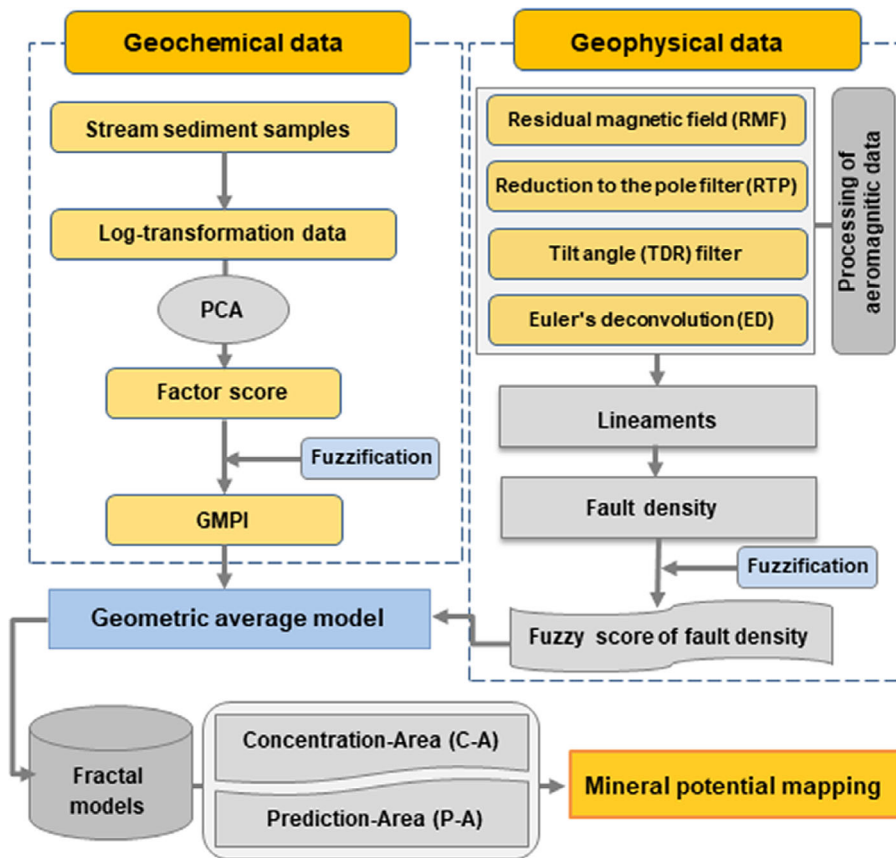


Figure 1. A schematic flowchart shows different layers and data of the prospectivity model used in the current study. The models incorporate geological, geochemical data from stream sediment samples and geophysical data to determine and identify anomalies associated with copper deposits. The geological layer is not shown in the flowchart for simplification.

Geological layer

The first data layer to be set in the study model is the geological layer (i.e., geological setting). The Tagmout basin, which is located in the Anti-Atlas Mountains, covers an area of 822 km² and is located in the northwestern Draa Basin of Eastern Morocco (Figure 2a). The Anti-Atlas consists of a series of inliers where igneous and metamorphic rocks of Paleoproterozoic and Neoproterozoic age are exposed (Kouyaté et al. 2013). Most of these inliers lie between or along the South Atlas Faults and the Anti-Atlas Major Fault (Figure 2a). The Proterozoic rocks were formed during the Paleoproterozoic Eburnian orogeny and the Neoproterozoic Pan-African orogeny. The Tagmout (or Tagmout Tin Ouayour) basin is located within the contact zone of the Ighrem inlier which is a basin characterized by abundant carbonate and siliciclastic formations (Figure 2b) (Pouclet et al. 2007). The basin was formed during the late stages of the Pan-African orogeny where extension occurred after accretion of volcanic arcs that once covered the entire Anti-Atlas range. The resulting basins have been interpreted to be pull-apart basins where siliciclastic sediments filled the basins (Pouclet et al. 2007). After the formation of the basins, a marine

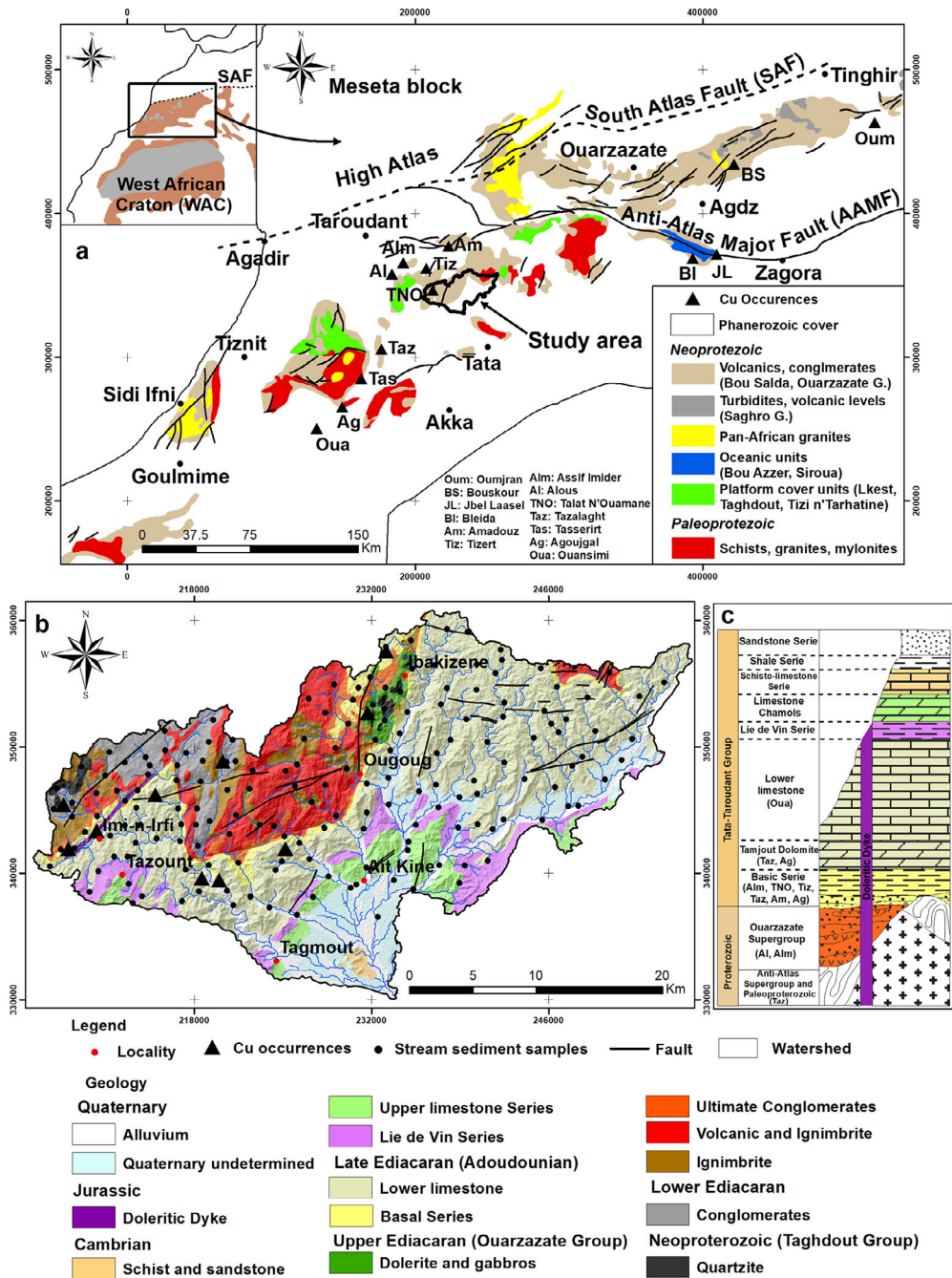


Figure 2. a. Geological map of the Anti-Atlas Mountains and surrounding regions. An outline shows the study area. Inset displays the location of the geological map in northwest Africa. SAF-South Atlas Fault. b. The geology map of the study shows the locations of the stream sediment sample and copper deposits. c. Lithostratigraphic column of Cambrian and Proterozoic formations and mineralization within each formation (adapted from Asladay et al. 1998).

transgression caused the deposition of carbonates during the Cambrian. Later Cambrian extension resulted in the deposition of transgressive sediments above the Cambrian sediments and Neoproterozoic lithologies (Poulet et al. 2007).

Proterozoic basement formations

The oldest lithostratigraphic unit within the study area is the Paleoproterozoic Zenaga Complex that forms a basement comprising granites, mica schists, sandstones, shales, and gneisses, where the siliciclastic and metamorphic rocks lie adjacent to the granites (Oudra et al. 2005). The Neoproterozoic rocks lie directly on top of the Paleoproterozoic units where the contact is considered to be tectonic since there is a brittle-ductile transition shear zone (Oudra et al. 2005). The Neoproterozoic rocks include Ourty Group overlain by Ighrem Group. The Ourty Group includes quartzites and carbonate units (Oudra 1988; Oudra et al. 2005), while the Ighrem Group is composed of conglomerates and volcano-detrital formations that were deposited in a basin formed during the later portions of the Pan-African orogeny (Oudra et al. 2005). The Upper Neoproterozoic is composed of conglomerates, sandstones, and volcanic units overlain by pelites and volcanic breccia (Choubert and Faure Muret 1973). The Upper Neoproterozoic rocks are directly located on quartzites of the Ourty Group (Oudra 1988).

Paleozoic units

The Paleozoic units lie unconformably over the Neoproterozoic rocks and include Adoudou and Lie-de-vin formations. The Adoudou Formation has been divided into several subunits including volcanoclastics and siliciclastic rocks of the Basal Series, and the overlying Lower Limestones which include the Tamjout Dolomite (Choubert 1963; Algouti et al. 2001; Benssaou and Hamoumi 2001) (Figure 2c). The Lie-de-vin Formation includes purplish-red pelites interspersed with carbonate beds and overlying subunits of the Upper Limestones and the schistose Limestone Series (Choubert 1963; Algouti et al. 2001; Benssaou and Hamoumi 2001). All of the above units have been dated to the Lower Cambrian (Choubert 1952; Boudda and Choubert 1972; Benziane et al. 1983; Benssaou and Hamoumi 2001) and were deposited in an intracontinental basin that formed during the rifting of the West African Craton (WAC) at the end of the Neoproterozoic (Soulaimani et al. 2003). Northeast-trending dolerite sills and dikes intrude all of the above units and are related to the opening of the Atlantic Ocean in the Triassic/Lias period (Sahabi et al. 2004).

Ore geology

The Anti-Atlas of Morocco has several world-class metallic ore deposits and over 200 known copper deposits that were formed by a variety of ore deposition mechanisms that include sedimentary exhalative deposits, vein deposits, volcanogenic massive sulfides, and epithermal processes (Bouabdellah and Slack 2016). The majority of these deposits are located within Neoproterozoic and Cambrian units overlying Paleoproterozoic rocks or along with the transition between these Neoproterozoic and the Cambrian units (Bourque et al. 2015). The copper mineralization is mostly epigenetic and is related to several tectonic events including rifting at the end of Proterozoic and compression during the Hercynian orogeny where a thermal event created conduits for the fluids or rifting during the Atlantic Ocean opening (Bouabdellah and Slack 2016).

There are 10 known copper deposits near and within the study area (Figure 2b). The most important copper deposits include the Alous, Assif Imider, Aménayo, Tizert, Amadou, Talat N'Ouamane, and Akiout deposits. These deposits are located within Late Neoproterozoic and Early Paleozoic lithologies. A number of these deposits occur within

or near volcanic structures (sills, intrusions, or dikes) which suggest a relationship between hydrothermal activity and later Neoproterozoic volcanic episodes or a margin basin (Pouit 1966; Chabane and Boyer 1979). The Tizert and Amadou copper deposits are emplaced within Cambrian lithologies and have a more controversial origin, but are more likely related to the Atlantic Ocean opening or Variscan compressional tectonics (e.g., Pouit 1966; Soulimani 1998; Oummouch et al. 2017). The Tizert and Amadou copper deposits were formed by synsedimentary processes (Bourque et al. 2015) within Late Ediacaran Basal Series sediments that are found within the Igherm inlier (Figure 2a) (Oummouch et al. 2017; Poot et al. 2020). The ore zones within the sedimentary rocks are 200 and 400 m below the surface and are located mostly along the Cambrian basin's margin adjacent to the Proterozoic basement highs (Oummouch et al. 2017). Additionally, the known mineralization occurrences are found near strike-slip faults that may have acted as a path for the ore-rich fluids (Oummouch et al. 2017) which deposited ore disseminated chalcopyrite, chalcocite, and bornite. Furthermore, the deposits have undergone supergene enrichment that formed significant deposits of azurite, malachite, and covellite (Poot et al. 2020).

The study area has several regions that contain polymetallic mineralization (Cu, Pb, and Zn) stratiform synsedimentary (Talat N'Ouamane). The mineralization is located within the Late Ediacaran Adoudou Formation either in the Base Series near the contact with the Precambrian substratum or higher in the carbonates bed of the Tamjout member. Rare occurrences are found in the Lower Limestone series, but they are always within the terrigenous facies with carbonates cement and/or in purely carbonates facies (Pouit 1966). The mineralization is present only in the base formation when its thickness reaches between 10 and 60 meters within low regions in the paleotopography of the underlying basement.

Spatial data

Stream sediment samples

Stream sediment samples were collected at 172 sites (Figure 2b) and were analyzed for their As, Cu, Pb, Ni, and Cr concentrations (Table 1). These elements are considered to be good indicators for potential copper deposits (Yang et al. 2009; Parsa et al. 2016). The sampling strategy and error-control procedures follow Johnson et al. (2001). Generally, only second and third-order tributaries were sampled (Figure 2b). Each sample consists of five samples collected along the stream's living bed. 2 to 5 cm of the surface layer is removed to avoid wind contamination. Dry sediments are sifted through a 2 mm mesh Nylon. The samples were analyzed by an X-ray fluorescence spectrometer (XRF) type Spectro X-LAB 2000. Quality control is done by inserting standard samples during each analysis session and randomly inserting control samples. The XRF ED is calibrated using several samples of international standards.

Geophysical data

Magnetic data were acquired in 1999 by Géoterrx-Dighem for the Moroccan Ministry of Energy and Mines. Flight lines were spaced 500 meters apart and were oriented N15° to N315°. The draped survey had an average ground clearance of 30 meters with the data collected using a cesium magnetometer that has a sensitivity of 0.01nT. The raw data were processed by removing noise and diurnal variations and detecting closing errors.

Table 1. Representative geochemical analyses of the studied stream sediments in ppm.

Sample	x	Y	As	Pb	Cu	Ni	Cr
AL11	231646.06283	347109.69684	43.00	0.00	24.00	27.00	48.00
AL15	230374.69677	338855.72313	28.00	0.00	23.00	27.00	43.00
AL21	233070.07435	352072.51020	0.00	0.00	21.00	52.00	143.00
AL28	227045.73950	353813.60256	27.00	0.00	19.00	26.00	52.00
AL3	230835.02067	339103.98360	47.00	0.00	33.00	26.00	46.00
AL30	232508.78450	336537.57442	34.00	0.00	18.00	26.00	45.00
AL33	245538.64616	344211.21757	37.00	0.00	17.00	29.00	40.00
CON16	221282.27516	344613.86045	33.00	0.00	24.00	33.00	67.00
CON2	208347.10026	345584.37012	7.00	0.00	57.00	50.00	138.00
CON23	220555.69196	348782.26024	14.00	0.00	21.00	50.00	110.00
CON25	221037.96695	350568.17100	17.00	0.00	21.00	42.00	94.00
CON30	215666.90647	351261.51878	26.00	0.00	19.00	47.00	108.00
CON4	208339.22920	344472.72821	25.00	0.00	50.00	33.00	76.00
CON40	220787.51904	343106.50280	30.00	0.00	18.00	25.00	43.00
CON42	224285.01035	343732.22306	36.00	0.00	18.00	29.00	62.00
CON49	214347.18266	347818.95701	21.00	0.00	17.00	55.00	123.00
DO237	223956.09876	337297.92247	52.00	9.00	19.00	26.00	29.00
DO243	239606.73534	359102.97567	46.00	10.00	59.00	35.00	66.00
DO245	235532.82067	343833.30960	36.00	10.00	23.00	28.00	42.00
DO270	228286.09250	343597.42135	52.00	12.00	19.00	26.00	44.00
DO272	242321.57675	356883.82676	42.00	13.00	34.00	38.00	75.00
DO273	241811.87767	355833.71226	43.00	13.00	29.00	35.00	60.00
DO29	242429.49366	352387.59869	59.00	0.00	27.00	31.00	44.00
DO3	233114.05081	354671.96480	0.00	0.00	23.00	46.00	160.00
DO300	233146.45899	357913.53519	33.00	17.00	50.00	33.00	60.00
DO309	215032.33627	342757.71427	44.00	18.00	127.00	28.00	37.00
DO310	220594.41168	338630.86016	41.00	18.00	48.00	28.00	43.00
DO311	245671.40172	352856.26683	45.00	18.00	28.00	30.00	46.00
DO314	241170.49699	350403.80884	67.00	19.00	43.00	31.00	43.00
DO319	221103.45062	337460.87603	40.00	20.00	58.00	28.00	40.00
DO323	248706.82782	349222.63174	45.00	20.00	22.00	31.00	48.00
DO325	216723.37325	345132.26050	37.00	21.00	43.00	31.00	49.00
DO327	222445.45268	338158.99604	43.00	21.00	23.00	28.00	41.00
DO330	238869.60452	343620.54102	45.00	22.00	23.00	34.00	52.00
DO331	237991.51336	359324.87600	43.00	23.00	35.00	32.00	57.00
DO332	211677.59086	341312.00019	47.00	23.00	25.00	27.00	33.00
DO353	246803.24190	351156.72551	71.00	28.00	33.00	23.00	14.00
DO354	212721.03690	341307.24153	39.00	28.00	29.00	30.00	44.00
DO355	216879.05051	342529.98698	53.00	29.00	33.00	27.00	34.00
DO363	213418.46011	345175.71490	46.00	41.00	125.00	26.00	34.00
DO364	206580.04350	340534.86850	47.00	44.00	33.00	36.00	61.00
DO366	217340.79932	340278.01384	38.00	50.00	29.00	32.00	48.00
DO370	213581.17066	343778.13917	42.00	161.00	102.00	24.00	22.00
DO40	233497.12917	349705.66309	15.00	0.00	22.00	41.00	79.00
DO45	241198.83197	340994.66239	35.00	0.00	21.00	31.00	41.00
DO5	234319.28079	354358.27206	0.00	0.00	21.00	51.00	191.00
DO53	248363.92161	345344.19821	23.00	0.00	18.00	65.00	79.00
DO54	233794.41557	339469.69173	24.00	0.00	17.00	26.00	48.00
DO6	232317.80125	350556.41980	0.00	0.00	12.00	52.00	172.00
DO65	242527.10977	353484.93802	58.00	1.00	27.00	31.00	51.00
GR42	229060.66717	354947.18108	28.00	0.00	11.00	18.00	30.00
GR45	222603.80214	348125.85413	23.00	1.00	20.00	28.00	51.00
GR46	242507.94354	348777.75931	51.00	2.00	26.00	27.00	37.00
GR5	230178.39115	351820.70337	26.00	0.00	29.00	25.00	51.00
GR53	247882.12587	348506.36215	54.00	19.00	21.00	30.00	39.00
GR54	230561.55850	353720.25069	7.00	53.00	31.00	29.00	84.00
GR55	208546.24418	341989.77903	25.00	97.00	137.00	25.00	44.00
GR56	216577.34699	347351.87368	16.00	0.00	108.00	37.00	85.00
GR60	210257.46004	346342.66407	23.00	0.00	13.00	45.00	141.00
GR63	209363.92926	343278.70003	2.00	0.00	34.00	18.00	34.00
GR67	221497.73963	340848.49951	31.00	0.00	18.00	27.00	42.00

(continued)

Table 1. Continued.

Sample	x	Y	As	Pb	Cu	Ni	Cr
GR69	231904.33132	355516.86665	36.00	3.00	60.00	30.00	59.00
GR70	226320.27206	342388.49213	50.00	23.00	20.00	28.00	44.00
Pel1	213510.61225	346547.90071	36.00	0.00	173.00	22.00	46.00
Pel12	211884.88542	346533.26927	27.00	0.00	17.00	28.00	47.00
Pel14	218235.42928	345106.13485	25.00	0.00	16.00	41.00	102.00
Pel15	235150.53551	358406.63636	13.00	0.00	16.00	55.00	148.00
SA24	249724.61149	351270.28305	43.00	26.00	22.00	28.00	35.00
SA3	250822.63452	355876.68810	22.00	0.00	18.00	28.00	53.00
SA7	255148.58067	355082.93651	22.00	0.00	16.00	28.00	53.00
SC1	212524.18046	345716.41561	10.00	0.00	115.00	30.00	64.00
SC12	210966.22887	347725.43403	31.00	0.00	13.00	45.00	118.00
SC2	209089.88098	348443.80297	19.00	0.00	78.00	49.00	114.00
SC3	206879.21672	345089.66986	32.00	0.00	76.00	47.00	125.00
SC5	232127.07979	353324.45382	3.00	0.00	36.00	53.00	196.00
SC6	233018.28488	353007.09441	8.00	0.00	27.00	50.00	148.00

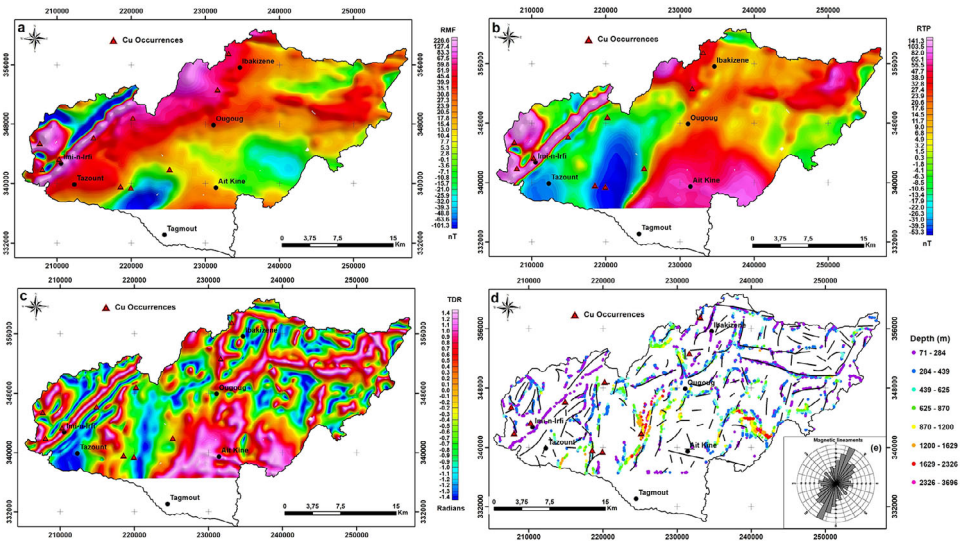


Figure 3. a. Residual magnetic anomaly (RMA) map. b. Reduction to the pole (RTP) of magnetic anomaly map. c. The tilt angle of the RTP data. d. Three-dimensional Euler deconvolution depths using a structural index of 0 superimposed the TDR angle derived lineaments. e. Rose diagram showing the orientation of the lineaments obtained the tilt angle method. Copper deposits are shown as triangles in Figures 3a, 3b, and 3c.

Additional data processing included removing the 1999 International Geomagnetic Reference Field (IGRF) to generate residual magnetic field data (RMF). The RMA map was digitized and gridded at a spacing of 125 m to produce RMF data (Figure 3a). To remove the dipolar effect of the Earth's magnetic field, the RMA data were reduced to pole (RTP) (Figure 3b) (Pham et al. 2020a, 2020b).

Fault data

The majority of the copper deposits within the Igherm inlier and surrounding areas are associated with faults that have acted as conduits for the passage of metal-rich fluids to upper crustal levels so they can be deposited in geochemical favorable regions (Levresse et al. 2016; Oummouch et al. 2017; Ouchchen et al. 2021). Thus, faults are an important

parameter in locating potential economic copper deposits. The known faults were digitized for their latitude and longitude from geological maps (Gasquet et al. 2008; Oummouch et al. 2017) (Figure 2a, 2b).

Data-driven methods

Factor analysis

Factor analysis (FA) is a multivariate analysis process (Afzal et al. 2016; Daviran et al. 2020; Ghezelbash et al. 2020) that can be used to generate significant multi-element anomalous signatures and to reduce the number of negative variables (Yousefi et al. 2012, 2014). Principal component analysis (PCA) can be used as a FA method with varimax rotation (Kaiser 1958) to reduce the number of variables in a dataset while preserving as much information about the dataset as possible (Filzmoser et al. 2009). During the PCA process, eigenvalues are calculated with the larger eigenvalues containing more variance (i.e., more information). While there are no specific techniques to determine how many eigenvalues to use in a study, Helvoort et al. (2005) and Yousefi et al. (2014) have shown that eigenvalues are greater than 1 contain sufficient information to be able to discriminate geochemical anomalies. Additionally, threshold values greater than 0.5 for loadings are considered sufficient to extract significant anomalous multi-element geochemical signatures (Yousefi et al. 2014). Factor analysis requires a normal or symmetrical data distribution; however, the stream sediment geochemical data are compositional and are not independent of each other (Filzmoser et al. 2009; Zuo et al. 2013). Thus, a log-transformation which is a normalization process was performed to generate symmetric data distributions (Cheng et al. 1994; Zuo 2011b; Wang et al. 2019).

Geochemical mineralization probably index of the geochemical anomalies

The stream sediment geochemistry was analyzed using the Geochemical Mineralization Probability Index (GMPI) was introduced by Yousefi et al. (2014) and is a probability method that develops classes using a stepwise FA. First, the distribution of geochemical anomalies is analyzed by determining their factorial scores (FS) and then, converted into an interval [0, 1] by applying a logistic function. This transformation of the stream sediment geochemical data into a logistic space generates a higher degree of differentiation between the geochemical anomalies and improves the forecast rate of potential mineral deposits (Parsa et al. 2016). The GMPI equation is:

$$GMPI = \frac{e^{FS}}{1 + e^{FS}} \quad (1)$$

where FS is the factor score of every sample used in the FA (Yousefi et al. 2012, 2014) and e is the exponential function. The GMPI of each multi-element association was then calculated.

Fuzzy weighting of fault density

Faults are an important component in determining the location of many ore deposits (Afzal et al. 2019). Faults and fractures can provide conduits for the movement of metal-rich fluids, circulation of hydrothermal fluids and will aid in determining the location of the ore deposits (Micklethwaite et al. 2010; Afzal et al. 2019). Thus, adding fault traces

determined from geological mapping or inferred from geophysical data to a data-driven database will increase the probability of locating ore deposits. Fault trace density (FD) was thus used to aid in predicting the location of ore deposits (Yousefi and Nykänen 2016). Several investigations have used a high FD as an indicator of copper mineralization (Pirajno 2010; Chen et al. 2011; Yousefi and Carranza 2015c).

To further analyze the FD data, a logistic function was used to convert continuous FD data to the range [0, 1] (Nykänen et al. 2008). By using the logistic conversion, the distinction between different classes of evidence data can be improved (Yousefi and Carranza 2015c). The following logistical transformation function was used to calculate FD values in a fuzzy space:

$$F_{FD} = \frac{1}{1 + e^{-s(FD-i)}} \quad (2)$$

Where F_{FD} and FD are the transformed values and values to be converted in the interval [0, 1] range, respectively (Yousefi and Carranza 2015c), i is the inflection point, and s is the slope. The i and s are defined by Yousefi and Nykänen (2016):

$$i = \frac{2 \ln 99}{\max(FD) - \min(FD)} \quad (3)$$

$$s = \frac{\max(FD) + \min(FD)}{2} \quad (4)$$

Using Equation (2), a fuzzy score map of the FD data was created (Figure 5).

Integration of weighted layers

In MPM, the integration of weighted evidence maps requires the use of functions that use a weight indicating the importance of each evidence map to provide the model that indicates the mineral potential target (Bonham-Carter 1994; Porwal et al. 2006; Ghezelbash et al. 2019a, 2019b). To accomplish this integration, we used the geometric average model to combine the map of fuzzy scores of two layers related to the significant mineralization, namely GMPI (Figure 5b) with the FD data (Figure 6), and to delineate the most prospective target zones for further exploration of the copper mineralization (Wang et al. 2007). The geometric average is the statistically average value when calculating a single average from several geodatabase evidential layers with geometrical support (Yousefi and Carranza 2015b). To calculate the geometric average function for copper mineralization, G_{ACu} , the following equation was used (Yousefi and Carranza 2015a):

$$G_{ACu}(F_{GMPI}, F_{FD}) = \left(\prod_{i=1}^2 F_i \right)^{1/2} = \sqrt{F_{GMPI} F_{FD}} \quad (5)$$

where F_{GMPI} and F_{FD} are the fuzzy scores of indicator values from the corresponding evidential maps, that were calculated using fuzzy operators (Parsa et al. 2016; Farahbakhsh et al. 2019; Roshanravan et al. 2020). The corresponding geometric average prospectivity map is shown in Figure 7a.

Table 2. Matrix of rotating components of the first and second steps.

First step			Second step			
Elements	F1	F2	F3	Elements	F1	F2
As	-0.816	0.119	-0.078	Pb	-0.535	0.625
Pb	-0.570	0.566	-0.526	Cu	-0.086	0.853
Cu	-0.147	0.833	0.531	Ni	0.881	0.333
Ni	0.799	0.430	-0.283	Cr	0.960	0.119
Cr	0.939	0.211	-0.063	Eigenvalues	1.991	1.243
Eigenvalues	2.532	1.259	0.649	Variance (%)	49.768	31.072
Variance (%)	50.646	25.175	12.975	Cumulative variance (%)	49.768	80.841
Cumulative variance (%)	50.646	75.821	88.795			

Creating evidence layers

Geochemical signature

A two-step FA was applied for extracting component stream sediment geochemical signatures. In the first step, factors F1 and F2 representing Ni–Cr and Cu–Pb multi-elements association, respectively, with positive loading are shown in Table 2. In the second step, As is considered to be a noisy element and was omitted from the dataset and further analysis. Therefore, the positive loads in F1 and F2 only take into account Ni–Cr and Cu–Pb multi-element association, respectively (Table 2). The total variance for the Ni–Cr association increased from 44.52% in the first-step F1 to 49.77% in the second-step F1, while variances for Cu–Pb increased from 27.63% in the first-step F2 to 31.07% in the second-step F2. Consequently, the FA successively reduced the number of factors and increased the intensity of the anomaly (as reported by Yousefi et al. 2012).

The FS obtained from the FA was used as a multi-element anomaly indicator. The FS has been used to create maps to identify geochemical anomalies that indicate mineralization or sources of geochemical contamination (Helvoort et al. 2005). FS values that have 95% of cumulative percentile as the background samples and threshold separating anomaly (Yousefi et al. 2014) were used in our analysis. The FS Ni–Cr (Figure 4a) and FS Cu–Pb (Figure 4b) distribution maps show the range of FS values within the Tagmout basin. The yellow to orange regions represent regions with anomalies that may contain higher levels of copper.

The distributions of the GMPI for the Cu–Pb and Ni–Cr associations are shown in Figure 5. To increase the intensity of the anomalies for copper mineralization, some multi-element associations can be omitted, even though they may be considered as evidence of copper mineralization. For this reason, the GMPI Ni–Cr results were excluded from our analysis, as they relate to certain lithological formations such as dolerite, gabbro, and quartzite, and the known copper deposits within the Anti-Atlas do not occur within these lithologies.

Faults density basing on magnetic data

The RTP signature of the Tagmout basin contains short and long wavelength anomalies with the highest amplitude anomalies occurring over possibly buried mafic Proterozoic rocks similar to those outcropping in the Igherm inlier (Ouchchen et al. 2021) in the southern portions of the study area (Figure 5b). Within the NW part of the study area, the northeast-trending magnetic maximum corresponds to a Jurassic-age dolerite dike, outcropping in the Ighrem inlier (Figure 2b). The other magnetic maxima located in the central and eastern parts of the study area also may be related to buried Proterozoic rocks but the linear nature of the central anomalies suggests that these may be related to linear structural features (i.e., fault systems). Magnetic data can help in determining lineaments

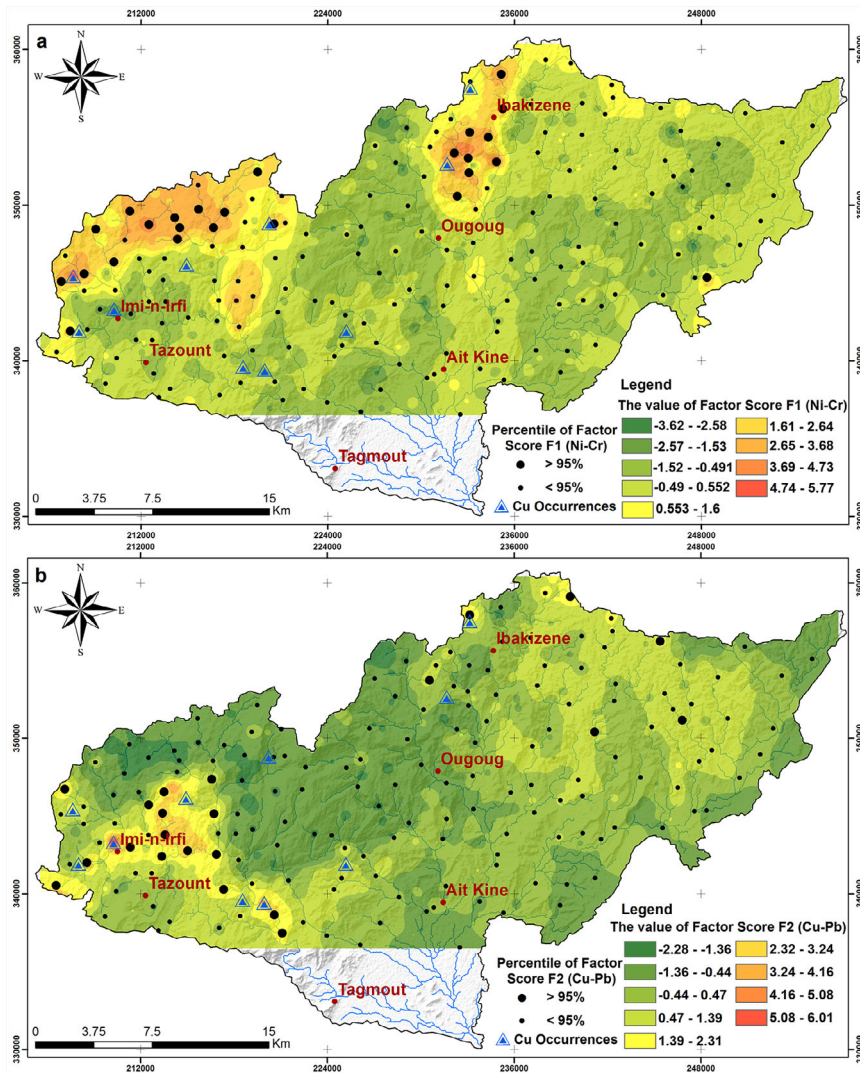


Figure 4. Factor score (FS) distribution of the stream sediment geochemistry data for Ni-Cr (a) and Cu-Pb (b).

with significant magnetization contrast (Salem et al. 2008) and therefore allow for a better understanding of the structural framework (Austin and Blenkinsop 2008, 2009; Salem et al. 2008; Henson et al. 2010; Pham et al. 2021b, 2021d). The cause of these lineaments could be the contact between rock units, faults, or fracture zones (Pham 2020, 2021d). To aid in determining lineaments within the magnetic data, derivative methods are commonly used including horizontal and vertical derivatives (Pham et al. 2021c, 2021d). Horizontal and vertical derivatives can produce large and small amplitude anomalies making interpretation of deeper sources difficult. Thus, the tilt angle derivative (TDR) was developed (Salem et al. 2008) which uses a ratio between the amplitudes of the vertical derivative and the total horizontal derivative that overcomes this problem. Figure 5c shows the TDR map of the RTP data.

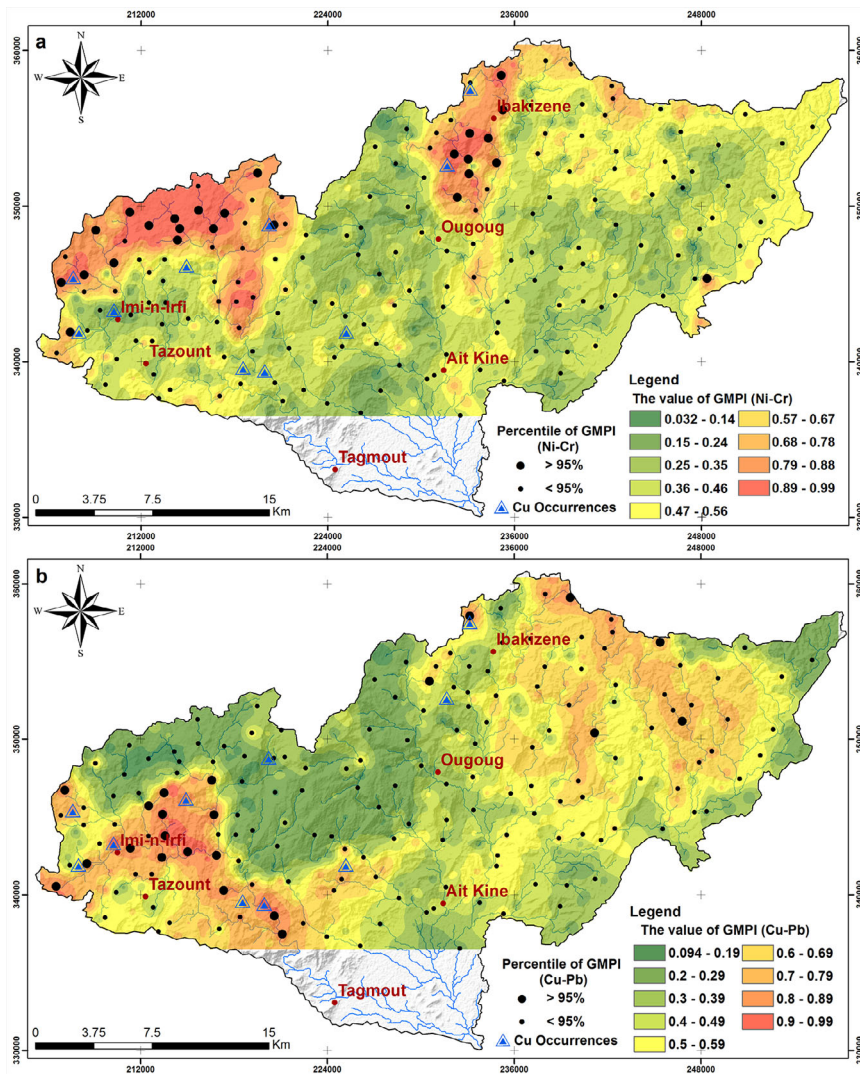


Figure 5. GMPI distribution of the stream sediment geochemistry data for Ni-Cr (a) and Cu-Pb (b).

Magnetic data can also be analyzed by performing a three-dimensional Euler's deconvolution analysis which is a derivative method but also allows determining the magnetic source depth (Reid et al. 1990). Euler deconvolution has several parameters that must be defined to get reliable results including window size, structural index (a model for the source geometry based on the dominant geology of the study area), and grid interval (Reid et al. 1990). We varied the window sizes between 5 and 20 km and consistently obtained similar depths for each window. A structural index of zero was used which corresponds to a thin sheet model. The TDR and Euler deconvolution analysis indicate lineaments trend NNE-SSW, NW-SE, and E-W with depths ranging from 90 to 2471 m (Figure 5c, 5d). A number of lineaments were observed near known copper deposits. The lineaments were deduced from the magnetic derivative analysis and were added to the fault database and integrated within the FD model.

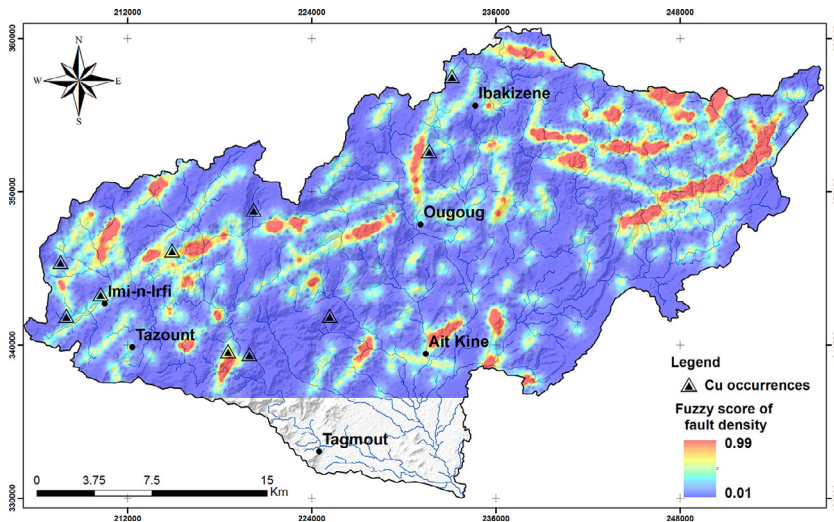


Figure 6. The fuzzy score of fault density (FD) is based on the mapped faults (Figure 2a) and magnetically derived lineaments (Figure 5d).

Evaluation of the geometric average prospectivity model

After the generation of the geometric average prospectivity models, the location of known mineral occurrences (Figure 2a) is used to evaluate the results. To do this procedure, the prospectivity model values must be classified using fractal operators (Meigoony et al. 2014; Yousefi and Carranza 2015a, 2015b; Afzal et al. 2016; Sanusi and Amigun 2020). For the Tagmout basin, the fractal concentration-area (C-A) model can be used to discriminate thresholds for classifying the prospectivity values (Cheng et al. 1994). In a log-log plot, a constant slope indicates a fractal dimension, so that the threshold values can be obtained as breakpoints in the plot (Nykänen et al. 2008). Based on Figure 7b, six classes or populations are obtained from the prospectivity model. The first four populations indicate low and medium concentration anomalies and the remaining populations indicate higher concentration anomalies. Based on these results, a classified map was generated (Figure 7c) with the highest intensity anomalies (>0.62) which are located in the northeast and west parts of the Tagmout basin.

For evaluating the importance of different classes, prediction-area (P-A; Parsa et al. 2016) plots were used. In a P-A plot, the intersection points of the curve of the cumulative percentage of known Cu occurrences and the curve of the cumulative percentage of prospectivity areas can be used as the prediction rate to evaluate the prospectivity model (Yousefi and Carranza 2015a, 2016). The prospectivity model can then be used to discriminate the further area for exploration (Yousefi and Carranza 2015a, 2015c). Based on Figure 7c and the location of the known mineral occurrences, P-A plots are then prepared (Figure 7d). The intersection point in Figure 7d shows that 55% of the known mineral occurrences are predicted within 45% of the Tagmout basin.

Yousefi and Carranza (2015a) proposed that the intersection point in a P-A plot can be used to determine two indexes: normalized density (Nd) and the weight of the targeting criterion (We) (Figure 7d). Nd is the prediction rate of a prospectivity map divided by its corresponding occupied area extracted from the intersection point of the P-A plot, while We, is the logarithm of Nd. These values can be interpreted as targeting criteria where $Nd > 1$ and $We > 0$ indicate that there is a positive association with the type of

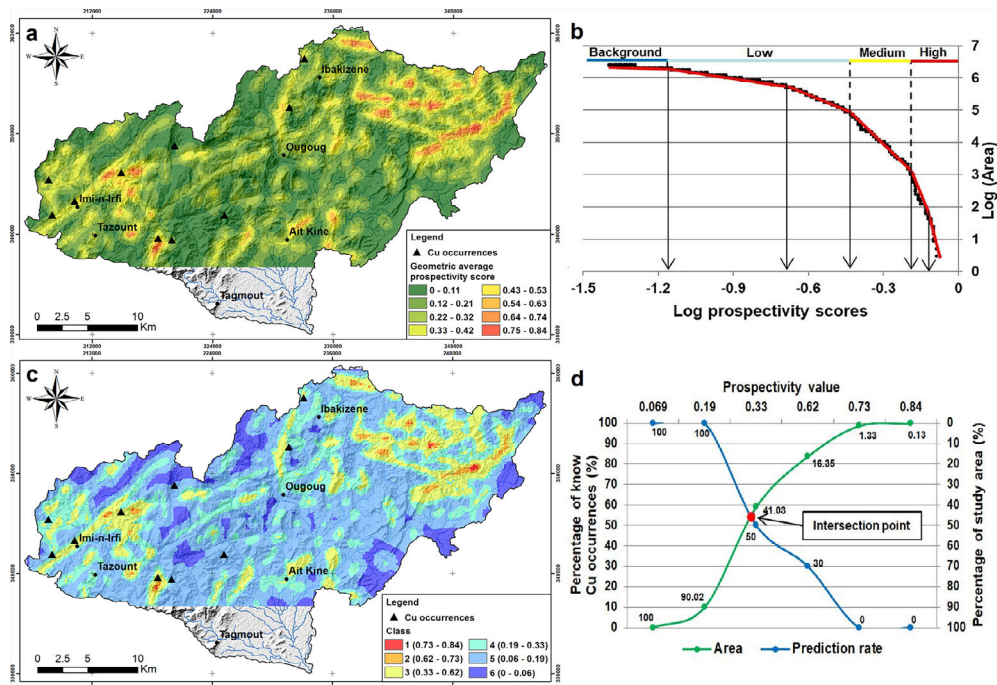


Figure 7. (a) Map of geometric averaged prospectivity scores generated by combining the fuzzy scores of FD (Figure 6) and GPMI CU-Pb results (Figure 5b). (b) Concentration–area fractal model (C–A) of the geometric averaged prospectivity results (Figure 7a). (c) Classification of copper-based on the C–A fractal model. (d) Prediction-area (P–A) plot of the classified geometric average prospectivity model.

deposit that is under investigation, while values $N_d < 1$ and $We < 0$ indicate that there is a negative association (Ghezelbash et al. 2019a). If $N_d = 1$ and $We = 0$, then the mineralization is independent of the targeting criteria (Ghezelbash et al. 2019a). Ghezelbash et al. (2019a) show that if the intersection point in a P–A plot has a higher value than other targeting criteria, then this targeting criterion is more effective than other targeting criteria in locating the desired mineralization. Thus, the two values can be used to prove the effectiveness of the selected model for the mineralization type (e.g., Mihalasky and Bonham-Carter 2001). The presented results indicate that $N_d = 1.22$ and $We = 0.20$ and suggest that the used prospectivity model is effective in locating copper mineralization. Figure 8 shows the regions which predict the locations of copper deposits within the Tagmout basin based on the presented models.

MPM: a technique for sustainable mineral exploration and mining activities - discussion

In MPM analyzes, the generation of target zones is an important step in a mineral exploration program, as the characteristics of a specific type of mineral deposit can be related to the geological features associated with the mineralization. It is generally accepted that fault zones are important conduits that promote the circulation of metal-bearing and hydrothermal fluids (Pirajno 2010) and have been found to be especially important in the Anti-Atlas Region of Morocco in locating and forming copper deposits (Ouchchen et al. 2021). One of the critical aspects in mineral prospecting is to determine the association between geochemical and geophysical anomalies, and geological features (Wang et al.

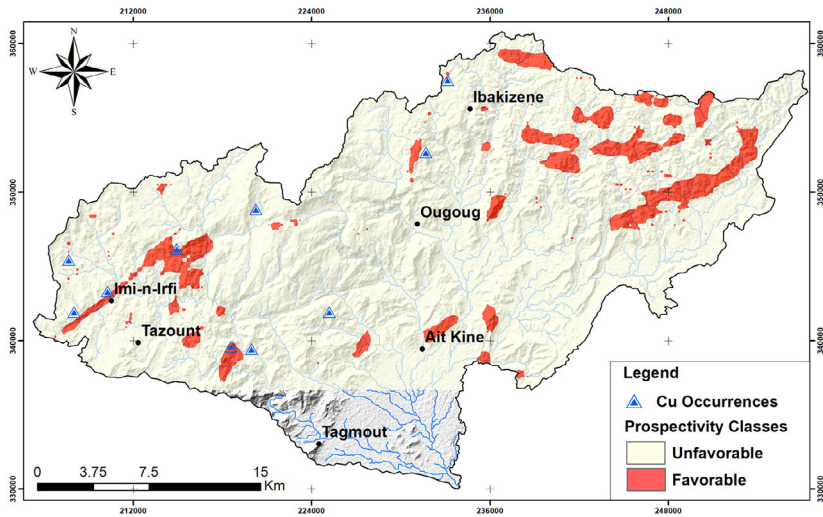


Figure 8. Delimited potential areas for further exploration of minerals.

2013). Yousefi et al. (2014), Yousefi and Nykänen (2016) and Yousefi and Carranza (2015a, 2016) have demonstrated that a combination of a set of effective layers of evidence of a certain type of ore deposit sought from different types of mineral exploration data (e.g., geochemical, geophysical, and geological) can be more reliable in targeting areas for more detailed exploration.

The spatial distribution of geochemical anomalies for a specific type of mineral deposit may differ from one area to another. Several geologically-based parameters that are related to the characteristics of a specific study area can be determined and may affect the spatial dispersion of certain geochemical elements (Spadoni 2006; Cheng 2007). For this reason, it is necessary to recognize that multi-elemental geochemical signatures may allow the delineation of anomalous zones. In this work, the multi-elemental Cu-Pb association has been found to have a good spatial relationship for the detection and predictor of the type of copper deposits found in the Tagmout basin. To generate an improved geochemical evidence map for MPM, the GMPI method was applied for the discrimination of anomalous copper zones, as it is a more powerful tool than an ordinary factor analysis for weighting and fuzzification of stream sediment geochemical data. As Yousefi et al. (2012, 2014) demonstrated, the transformation of geochemical signatures using a logistic function of FS increases the prediction rate of MPM and allows for better discrimination of geochemical populations compared to a factor score alone. The GMPI results based on an indicator component can then be considered as values of significant geochemical anomalous for the enhancement of exploration success. As can be seen in Figure 5, the area with known copper occurrences within the Tagmout basin has a high intensity of GMPI, but in the northeast portions of the basin without any known copper deposits also have a high intensity of GMPI. This portion of the basin should be considered a potential area for further mineral exploration, as it indicates promising new regions, which have not been previously determined by individual indicator components. Based on the geological map (Figure 2b), the GMPI and the Cu-Pb anomalies occurring in the western portions of the Tagmout basin are lithology related, as they correlate with the Basic series and the contact zones between the limestone and basement. The majority of the copper deposits in the Tagmout basin and surrounding area are located in these geological units

(Bouabdellah and Slack 2016) and whose origin was controlled by the NE-SW trending faults (Ouchchen et al. 2021). GMPI and Cu-Pb anomalies were also determined within the northeastern portion of the Tagmout basin and can be correlated with the E-W and NE-SW trending lineaments determined by magnetic tilt angle analysis (Figure 3c).

Fuzzy operators were applied to weight effective geochemical evidence layers and FD data (Figures 5b and 6). The spatial evidence values that come from different datasets are converted to the same data space from 0 to 1 which facilitates their integration for further analysis. Each of the maps generated in this work can be used in the mineral prospectivity modeling of copper deposits through the application of the geometric average model, which permits the delimitation of reliable target areas for mineral exploration. To estimate the ability of the generated mineral prospecting model to discriminate copper mineralization zones, the normalized density index (Nd) and the P-A were used to detect threshold values (Figure 7d). Our analysis indicated that the value of 0.31 was determined as the threshold for the validation of the prospectivity map (Figure 8). Thus, the determined Nd value shows that the applied prospectivity model is also efficient because Nd is >1 and the corresponding We values are positive. These results show that areas with high prospectivity values can be used as targets for further exploration within the Tagmout basin. Figure 8 shows that the target areas produced by using the geometric average function represent an area of 8.22% of the Tagmout basin that may contain significant copper occurrences with 30% of these being concentrated in the western part of the basin. These values indicate that the integrated layers have a strong spatial correlation with the known copper occurrences locations. These potential copper mineralization areas trend E-W and NE-SW near similarly trending known faults and magnetically determined lineaments. These potential copper mineralization areas are mostly located in the western, northeast, and southwest portions of the Tagmout basin.

The results of the current study can be used to define future exploration programs in the western, southwestern, and northeastern portions of the Tagmout basin which give a sustainable perspective of copper exploration and mining activities in Morocco. The data needed to run similar sustainability evaluations are stream sediment geochemical data, whole-rock geochemical data, detailed geological mapping including lithological mapping, fault analysis, and hydrothermal alteration mapping, and detailed geophysical exploration. The geophysical methods may include magnetic, airborne electromagnetic surveys, electrical resistivity, and ground electromagnetics.

Conclusions

Stream sediment geochemical, aeromagnetic, and geological data were analyzed in the Tagmout basin within the Anti-Atlas region of western Morocco to determine favorable locations for more detailed exploration for copper exploration. The datasets were analyzed using mineral prospectivity mapping based on the principle of the geometric mean. The input data to MPM was processed using fuzzy operators within a factor analysis on the stream sediment geochemical data and fault density data. The fault density data were determined from geological mapping and magnetic lineaments derived from a tilt angle analysis of the reduction to the pole aeromagnetic data. The MPM function using the fuzzy analysis results determined the most favorable regions of potential copper mineralization for future exploration activities. These potential copper mineralization regions were further analyzed to determine the accuracy of the MPM model. The accuracy as indicated by the normalized density index was 1.22. This value suggests that the suggested copper mineralization areas are statistically reliable.

The MPM model suggests that 8.22% of the Tagmout basin contains significant concentrations of copper mineralization. Out of this percentage, 30% occurs in the western Tagmout basin. The northeastern and southwestern portions of the basin also contain significant amounts of copper mineralization. These mineralization zones lie along east- and northeast-trending regions and are parallel to known faults and magnetic lineaments in the region. Faults are important for copper mineralization in the western Anti-Atlas since they facilitate the circulation of copper-bearing fluid from deeper crustal levels upward to the favorable lithology for precipitation. The MPM modeling succeeded to predict the locations of well-known copper deposits in the western part of the Tagmout basin and suggests other potential regions in the northeastern and southwestern of the basin for further exploration activities which indicate that the MPM is a potential technique for sustainable mineral exploration and mining activities.

Acknowledgments

Our deepest gratitude to Professor Bradley C. Rundquist (Editor-In-Chief, *Geocarto International*) and three anonymous reviewers for their careful work and thoughtful suggestions that have helped improve this paper substantially. This paper is a contribution to IGCP 683: "Pre-Atlantic geological connections among northwest Africa, Iberia and eastern North America: Implications for continental configurations and economic resources". All authors approved the final version of the manuscript.

Ethical statement

The authors declare that all ethical practices have been followed in relation to the development, writing, and publication of the article.

Disclosure statement

No potential conflict of interest was reported by the authors.

Funding

This research received no specific grant from any funding agency in the public, commercial, or not-for-profit sectors.

Data availability statement

The data that support the findings of this study are available from the corresponding author, upon reasonable request.

References

- Afzal P, Khakzad A, Moarefvand P, Omran NR, Esfandiari B, Alghalandis YF. 2010. Geochemical anomaly separation by multifractal modeling in Kahang (Gor Gor) porphyry system, Central Iran. *J Geochem Explor.* 104(1-2):34–46.
- Afzal P, Mirzaei M, Yousefi M, Adib A, Khalajmasoumi M, Zarifi AZ, Foster P, Yasrebi AB. 2016. Delineation of geochemical anomalies based on stream sediment data utilizing fractal modeling and staged factor analysis. *J Afr Earth Sci.* 119:139–149.
- Afzal P, Yousefi M, Mirzaie M, Ghadiri-Sufi E, Ghasemzadeh S, Daneshvar Saein L. 2019. Delineation of podiform-type chromite mineralization using geochemical mineralization prospectivity index and staged factor analysis in Balvard area (SE Iran). *J Min Env.* 10(3):705–715.

- Algouti A, Algouti A, Chbani B, Zaim M. 2001. Sedimentation et volcanisme synsédimentaire de la série de base de l'Adoudounien infra-cambrien à travers deux exemples de l'Anti-Atlas du Maroc [Sedimentation and syn-sedimentary volcanism of the infra-Cambrian Adoudounian Basal series interpreted from two areas in the Moroccan Anti-Atlas mountains]. *J Afr Earth Sci.* 32(4):541–556.
- Almasi A, Jafarirad A, Afzal P, Rahimi M. 2015. Prospecting of gold mineralization in Saqez area (NW Iran) using geochemical, geophysical and geological studies based on multifractal modelling and principal component analysis. *Arab J Geosci.* 8(8):5935–5947.
- Asladay A, Barodi EB, Maacha L, Zinbi Y. 1998. Les minéralisations cuprifères du Maroc. *Chron Rech Min.* 531-532:29–44.
- Austin JR, Blenkinsop TG. 2008. The Cloncurry lineament: geophysical and geological evidence for a deep crustal structure in the Eastern Succession of the Mount Isa Inlier. *Precambrian Res.* 163(1-2): 50–68.
- Austin JR, Blenkinsop TG. 2009. Local to regional scale structural controls on mineralisation and the importance of a major lineament in the eastern Mount Isa Inlier, Australia: review and analysis with autocorrelation and weights of evidence. *Ore Geol Rev.* 35(3-4):298–316.
- Benssaou M, Hamoumi N. 2001. L'Anti-Atlas occidental du Maroc: étude sédimentologique et reconstitutions paléogéographiques au Cambrien inférieur [The western Anti-Atlas of Morocco: sedimentological and palaeogeographical formation studies in the Early Cambrian]. *J Afr Earth Sci.* 32(3):351–372.
- Benziane F, Yazidi A, Prost AE. 1983. Le passage du précambrien, le Cambrien précoce volcanique et sédimentaire de l'Anti-Atlas oriental, comparaisons avec l'Anti-Atlas occidental [The transition from the latest Precambrian to the volcanic and sedimentary early Cambrian of the eastern Anti-Atlas; comparisons with the western Anti-Atlas]. *Bull Soc Geol Fr.* 7(4):549–556.
- Bonham-Carter GF. 1994. *Geographic information systems for geoscientists: Modelling with GIS.* 1st ed. Oxford: Pergamon.
- Bonham-Carter GF, Agterberg FP, Wright DF. 1989. Weights of evidence modelling: A new approach to mapping mineral potential. In: Agterberg FP, Bonham-Carter GF, editors. *Statistical applications in the earth sciences.* Ottawa: Geological Survey of Canada (Paper no. 89-9); p. 171–183.
- Bouabdellah M, Slack J. 2016. Geologic and metallogenic framework of North Africa. In: Bouabdellah M, Slack J, editors. *Mineral Deposits of North Africa.* Cham: Springer; p. 3–81.
- Boudda A, Choubert G. 1972. Sur la limite inférieure du Cambrien au Maroc. *CR Acad Sci Paris.* 275: 5–8.
- Bourque H, Barbanson L, Sizaret S, Branquet Y, Ramboz C, Ennaciri A, El Ghorfi M, Badra L. 2015. Contribution to the synsedimentary versus epigenetic origin of the Cu mineralizations hosted by terminal Neoproterozoic to Cambrian formations of the Bou Azzer-El Graara inlier: New insights from the Jbel Laassel deposit (Anti Atlas, Morocco). *J Afr Earth Sci.* 107:108–118.
- Carranza EJM. 2010. Catchment basin modelling of stream sediment anomalies revisited: incorporation of EDA and fractal analysis. *Geochem Explor Environ Anal.* 10(2):171–187.
- Carranza EJM, Sadeghi M. 2010. Predictive mapping of prospectivity and quantitative estimation of undiscovered VMS deposits in Skellefte district (Sweden). *Ore Geol Rev.* 38(3):219–241.
- Carranza EJM, van Ruitenbeek FJA, Hecker C, van der Meijde M, van der Meer FD. 2008. Knowledge-guided data-driven evidential belief modeling of mineral prospectivity in Cabo de Gata, SE Spain. *Int J Appl Earth Obs Geoinf.* 10(3):374–387.
- Chabane A, Boyer C. 1979. Séries volcaniques et minéralisations cuprifère du Précambrien supérieur de Tanguerfa, Anti-Atlas, Maroc. *CR Acad Sci Paris.* 288(1):5–8.
- Chen Z, Zhang L, Wan B, Wu H, Cleven N. 2011. Geochronology and geochemistry of the Wunugetushan porphyry Cu-Mo deposit in NE China, and their geological significance. *Ore Geol Rev.* 43(1):92–105.
- Cheng Q. 2007. Mapping singularities with stream sediment geochemical data for prediction of undiscovered mineral deposits in Gejiu, Yunnan Province, China. *Ore Geol Rev.* 32(1-2):314–324.
- Cheng Q, Agterberg FP, Ballantyne SB. 1994. The separation of geochemical anomalies from background by fractal methods. *J Geochem Explor.* 51(2):109–130.
- Choubert G. 1963. Essai de mise au point du problème des "ignimbrites". *Bull Volcanol.* 25(1):123–140.
- Choubert G, Clariond L, Hindermeyer J. 1952. *Livret-guide de l'excursion C36: Anti-Atlas central et oriental.* Congrès Géologique International, XIXe session-Alger-1952, Série: Maroc. 11:89–98.
- Choubert G, Faure Muret A. 1973. Nouvelles données sur les massifs précambriens des Ida Ou-Zeddoute et des Ida Ou-Zekri, NW d'Igherm, Anti-Atlas (Maroc). *CR Acad Sci Paris.* 276(4):477–480.
- Daviran M, Maghsoudi A, Cohen DR, Ghezlbash R, Yilmaz H. 2020. Assessment of Various Fuzzy c-Mean Clustering Validation Indices for Mapping Mineral Prospectivity: Combination of Multifractal Geochemical Model and Mineralization Processes. *Nat Resour Res.* 29(1):229–246.

- Farahbakhsh E, Chandra R, Eslamkish T, Müller RD. 2019. Modeling geochemical anomalies of stream sediment data through a weighted drainage catchment basin method for detecting porphyry Cu-Au mineralization. *J Geochem Explor.* 204:12–32.
- Filzmoser P, Hron K, Reimann C. 2009. Principal components analysis for compositional data with outliers. *Environmetrics.* 20(6):621–632.
- Gasquet D, Ennih N, Liégeois JP, Soulaïmani A, Michard A. 2008. The Pan-African belt. In: Michard A, Saddiqi O, Chalouan A, Frizon Lamotte D, editors. *Continental evolution: The geology of Morocco.* Cham: Springer; p. 33–64.
- Ghezelbash R, Maghsoudi A, Carranza EJM. 2019a. An improved data-driven multiple criteria decision-making procedure for spatial modeling of mineral prospectivity: adaption of prediction–area plot and logistic functions. *Nat Resour Res.* 28(4):1299–1316.
- Ghezelbash R, Maghsoudi A, Carranza EJM. 2019b. Performance evaluation of RBF-and SVM-based machine learning algorithms for predictive mineral prospectivity modeling: integration of SA multifractal model and mineralization controls. *Earth Sci Inform.* 12(3):277–293.
- Ghezelbash R, Maghsoudi A, Carranza EJM. 2020. Sensitivity analysis of prospectivity modeling to evidence maps: Enhancing success of targeting for epithermal gold, Takab district, NW Iran. *Ore Geol Rev.* 120:103394.
- Helvoort PJ, Filzmoser P, Gaans PFM. 2005. Sequential Factor Analysis as a new approach to multivariate analysis of heterogeneous geochemical datasets: an application to a bulk chemical characterization of fluvial deposits (Rhine–Meuse delta, The Netherlands). *Appl Geochem.* 20(12):2233–2251.
- Henson P, Blewett R, Roy I, Miller J, Czarnota K. 2010. 4 D architectures and tectonic evolution of the Laverton region, eastern Yilgarn Craton, West Australia. *Precambrian Res.* 183(2):338–355.
- Johnson CC, Flight DMA, Lister TR, Strutt MH. 2001. Le rapport final pour les travaux de recherches géologique pour la réalisation de cinq cartes géochimiques au 1/100 000 dans le domaine de l'Anti-Atlas (Maroc). Keyworth, Nottingham: British Geological Survey. Commissioned Report Series, CR/01/031.
- Kaiser HF. 1958. The varimax criteria for analytical rotation in factor analysis. *Psychometrika.* 23(3): 187–200.
- Kouhestani H, Ghaderi M, Afzal P, Zaw K. 2020. Classification of pyrite types using fractal and stepwise factor analyses in the Chah Zard gold-silver epithermal deposit, central Iran. *Geochem Explor Environ Anal.* 20(4):496–508.
- Kouyaté D, Söderlund U, Youbi N, Ernst R, Hafid A, Ikenne M, Soulaïmani A, Bertrand H, El Janati M, R'kha Chaham K. 2013. U-Pb baddeleyite and zircon ages of 2040 Ma, 1650 Ma and 885 Ma on dolerites in the West African Craton (Anti-Atlas inliers): Possible links to break up of Precambrian supercontinents. *Lithos.* 174:71–84.
- Levesse G, Bouabdellah M, Cheilletz A, Gasquet D, Maacha L, Tritlla J, Banks D, Samir Mr A. 2016. Degassing as the main ore-forming process at the giant Imiter Ag-Hg vein deposit in the Anti-Atlas Mountains, Morocco. In: Bouabdellah M, Slack J, editors. *Mineral deposits of North Africa.* Cham: Springer; p. 85–106.
- Mandelbrot BB. 1983. *The fractal geometry of nature.* New York (NY): W. H. Freeman and Company.
- Meigoony MS, Afzal P, Gholinejad M, Yasrebi AB, Sadeghi B. 2014. Delineation of geochemical anomalies using factor analysis and multifractal modeling based on stream sediments data in Sarajeh 1: 100,000 sheet, Central Iran. *Arab J Geosci.* 7(12):5333–5343.
- Micklethwaite S, Sheldon HA, Baker T. 2010. Active fault and shear processes and their implications for mineral deposit formation and discovery. *J Struct Geol.* 32(2):151–165.
- Mihalasky MJ, Bonham-Carter GF. 2001. Lithodiversity and its spatial association with metallic mineral sites, Great Basin of Nevada. *Nat Resour Res.* 10(3):209–226.
- Nykänen V, Groves DI, Ojala VJ, Eilu P, Gardoll SJ. 2008. Reconnaissance-scale conceptual fuzzy-logic prospectivity modelling for iron oxide copper-gold deposits in the northern Fennoscandian Shield, Finland. *Aust J Earth Sci.* 55(1):25–38.
- Ouchchen M, Boutaleb S, Abia EH, El Azzab D, Abioui M, Mickus KL, Miftah A, Echogdali FZ, Dadi B. 2021. Structural interpretation of the Igherm region (Western Anti Atlas, Morocco) from an aeromagnetic analysis: Implications for copper exploration. *J Afr Earth Sci.* 176:104140.
- Oudra M. 1988. *La structuration panafricaine dans la partie nord-ouest de la boutonnière d'Irhem (Anti-Atlas occidental-Maroc)[dissertation].* Marrakech: Cadi Ayyad University.
- Oudra M, Beraaouz H, Ikenne M, Gasquet D, Soulaïmani A. 2005. La tectonique panafricaine du secteur d'Igherm: implication des dômes extensifs tardi à post-orogéniques (Anti-Atlas occidental, Maroc). *Estud Geol.* 61(3-6):177–189.

- Oummouch A, Essaifi A, Zayane R, Maddi O, Zouhair M, Maacha L. 2017. Geology and metallogenesis of the sediment-hosted Cu-Ag deposit of Tizert (Igherm inlier, Anti-Atlas Copperbelt, Morocco). *Geofluids*. 2017:7508484.
- Parsa M, Maghsoudi A, Yousefi M, Sadeghi M. 2016. Prospectivity modeling of porphyry-Cu deposits by identification and integration of efficient mono-elemental geochemical signatures. *J Afr Earth Sci*. 114: 228–241.
- Pham LT. 2020. A comparative study on different filters for enhancing potential field source boundaries: synthetic examples and a case study from the Song Hong Trough (Vietnam). *Arab J Geosci*. 13(15): 723.
- Pham LT. 2021. A high resolution edge detector for interpreting potential field data: A case study from the Witwatersrand basin, South Africa. *J Afr Earth Sci*. 178:104190.
- Pham LT, Eldosouky AM, Oksum E, Saada SA. 2020a. A new high-resolution filter for source edge detection of potential data. *Geocarto Int*. 1–18. DOI:10.1080/10106049.2020.1849414
- Pham LT, Oksum E, Do TD, Nguyen DV, Eldosouky AM. 2021a. On the performance of phase-based filters for enhancing lateral boundaries of magnetic and gravity sources: a case study of the Seattle Uplift. *Arab J Geosci*. 14(2):129.
- Pham LT, Oksum E, Le DV, Ferreira FJF, Le ST. 2021b. Edge detection of potential field sources using the softsign function. *Geocarto Int*. 1–14. DOI:10.1080/10106049.2021.1882007
- Pham LT, Oksum E, Vu MD, Vo QT, Le-Viet KD, Eldosouky AM. 2021c. An improved approach for detecting ridge locations to interpret the potential field data for more accurate structural mapping: a case study from Vredefort dome area (South Africa). *J Afr Earth Sci*. 175:104099.
- Pham LT, Vu MD, Le ST. 2021d. Performance evaluation of amplitude- and phase-based methods for estimating edges of potential field sources. *Iran J Sci Technol Trans Sci*. 45(4):1327–1339.
- Pham LT, Vu TV, Le-Thi S, Trinh PT. 2020b. Enhancement of potential field source boundaries using an improved logistic filter. *Pure Appl Geophys*. 177(11):5237–5249.
- Pirajno F. 2010. Intracontinental strike-slip faults, associated magmatism, mineral systems and mantle dynamics: Examples from NW China and Altay-Sayan (Siberia). *J Geodyn*. 50(3-4):325–346.
- Poot J, Verhaert M, Dekoninck A, Oummouch A, El Basbas A, Maacha L, Yans J. 2020. Characterization of weathering processes of the giant copper deposit of Tizert (Igherm Inlier, Anti-Atlas, Morocco). *Minerals*. 10(7):620.
- Porwal A, Carranza EJM, Hale M. 2006. A hybrid fuzzy weights-of-evidence model for mineral potential mapping. *Nat Resour Res*. 15(1):1–14.
- Pouclot A, Aarab A, Fekkak A, Benharref M. 2007. Geodynamic evolution of the northwestern Paleogondwanan margin in the Moroccan Atlas at the Precambrian-Cambrian boundary. In: Linnemann U, Nance R, Kraft P, Zulauf G, editors. *The evolution of the Rheic Ocean: From Avalonian-Cadomian active margin to Alleghenian-Variscan collision*, Vol. 423. Boulder: Geol Soc Am Spec Pap.; p. 27–60.
- Pouit G. 1966. Paléogéographie et répartition des minéralisations stratiformes de cuivre dans l'Anti-Atlas occidental. *Chron Rech Min*. 34(356):279–289.
- Pourgholam MM, Afzal P, Yasrebi AB, Gholinejad M, Wetherelt A. 2021. Detection of geochemical anomalies using a fractal-wavelet model in Ipack area, Central Iran. *J Geochem Explor*. 220:106675.
- Reid AB, Allsop JM, Granser H, Millett AT, Somerton IW. 1990. Magnetic interpretation in three dimensions using Euler deconvolution. *Geophysics*. 55(1):80–91.
- Roshanravan B, Kreuzer OP, Bruce M, Davis J, Briggs M. 2020. Modelling gold potential in the Granites-Tanami Orogen, NT, Australia: a comparative study using continuous and data-driven techniques. *Ore Geol Rev*. 125:103661.
- Sahabi M, Aslanian D, Olivet JL. 2004. Un nouveau point de départ pour l'histoire de l'Atlantique central [A new starting point for the history of the central Atlantic]. *CR Geosci*. 336(12):1041–1052.
- Salem A, Williams S, Fairhead D, Smith R, Ravat D. 2008. Interpretation of magnetic data using tilt-angle derivatives. *Geophysics*. 73(1):L1–L10.
- Sanusi SO, Amigun JO. 2020. Logistic-based translation of orogenic gold forming processes into mappable exploration criteria for fuzzy logic mineral exploration targeting in the Kushaka Schist Belt, North-Central Nigeria. *Nat Resour Res*. 29(6):3505–3526.
- Shahbazi S, Ghaderi M, Afzal P. 2021. Prognosis of gold mineralization phases by multifractal modeling in the Zehabad epithermal deposit, NW Iran. *Iran J Earth Sci*. 13(1):31–40.
- Shamseddin Meigooni M, Lotfi M, Afzal P, Nezafati N, Kargar Razi M. 2021. Application of multivariate geostatistical simulation and fractal analysis for detection of rare earth elements (REEs) geochemical anomalies in Esfordi phosphate mine, Central Iran. *Geochem Explor Environ Anal*. 21(2):1–17.
- Soulaimani A. 1998. Interactions socle/couverture dans l'Anti-Atlas occidental (Maroc): rifting fini-Protérozoïque et orogénèse hercynienne [dissertation]. Marrakech: Caddi Ayyad University.

- Soulaimani A, Bouabdelli M, Piqué A. 2003. L'extension continentale au Néoproterozoïque supérieur-Cambrien inférieur dans l'Anti-Atlas (Maroc)[The Upper Neoproterozoic-Lower Cambrian continental extension in the Anti-Atlas (Morocco). *Bull Soc Geol Fr.* 174(1):83–92. French.
- Spadoni M. 2006. Geochemical mapping using a geomorphologic approach based on catchments. *J Geochem Explor.* 90(3):183–196.
- Wang C, Carranza EJM, Zhang S, Zhang J, Liu X, Zhang D, Sun X, Duan C. 2013. Characterization of primary geochemical haloes for gold exploration at the Huanxiangwa gold deposit, China. *J Geochem Explor.* 124:40–58.
- Wang X, Xia Q, Li T, Leng S, Li Y, Kang L, Chen Z, Wu L. 2019. Application of fractal models to delineate mineralized zones in the Pulang porphyry copper deposit, Yunnan, southwestern China. *Nonlin Processes Geophys.* 26(3):267–282.
- Wang YM, Chin KS, Yang JB. 2007. Measuring the performances of decision making units using geometric average efficiency. *J Oper Res Soc.* 58(7):929–937.
- Wu JZ, Zhang Q. 2011. Multicriteria decision making method based on intuitionistic fuzzy weighted entropy. *Expert Syst Appl.* 38(1):916–922.
- Xu Z, Cai X. 2010. Recent advances in intuitionistic fuzzy information aggregation. *Fuzzy Optim Decis Making.* 9(4):359–381.
- Yousefi M, Carranza EJM. 2015a. Geometric average of spatial evidence data layers: A GIS based multicriteria decision-making approach to mineral prospectivity mapping. *Comput Geosci.* 83:72–79.
- Yousefi M, Carranza EJM. 2015b. Prediction–area (P–A) plot and C–A fractal analysis to classify and evaluate evidential maps for mineral prospectivity modeling. *Comput Geosci.* 79:69–81.
- Yousefi M, Carranza EJM. 2015c. Fuzzification of continuous-value spatial evidence for mineral prospectivity mapping. *Comput Geosci.* 74:97–109.
- Yousefi M, Carranza EJM. 2016. Data driven index overlay and Boolean logic mineral prospectivity modeling in Greenfields exploration. *Nat Resour Res.* 25(1):3–18.
- Yousefi M, Nykänen V. 2016. Data-driven logistic-based weighting of geochemical and geological evidence layers in mineral prospectivity mapping. *J Geochem Explor.* 164:94–106.
- Yousefi M, Kamkar-Rouhani A, Carranza EJM. 2012. Geochemical mineralization probability index (GMPI): a new approach to generate enhanced stream sediment geochemical evidential map for increasing probability of success in mineral potential mapping. *J Geochem Explor.* 115:24–35.
- Yousefi M, Kamkar-Rouhani A, Carranza EJM. 2014. Application of staged factor analysis and logistic function to create a fuzzy stream sediment geochemical evidence layer for mineral prospectivity mapping. *Geochem Explor Environ Anal.* 14(1):45–58.
- Yang Z, Hou Z, White NC, Chang Z, Li Z, Song Y. 2009. Geology of the post-collisional porphyry copper-molybdenum deposit at Qulong, Tibet. *Ore Geol Rev.* 36(1-3):133–159.
- Zadeh LA. 1965. Fuzzy sets. *Inf Control.* 8(3):338–353.
- Zhang X, Liu P. 2010. Method for aggregating triangular fuzzy intuitionistic fuzzy information and its application to decision making. *Technol Econ Dev Econ.* 16(2):280–290.
- Zuo R. 2011a. Decomposing of mixed pattern of arsenic using fractal model in Gangdese belt, Tibet, China. *Appl Geochem.* 26:S271–S273.
- Zuo R. 2011b. Identifying geochemical anomalies associated with Cu and Pb-Zn skarn mineralization using principal component analysis and spectrum–area fractal modeling in the Gangdese Belt, Tibet (China). *J Geochem Explor.* 111(1-2):13–22.
- Zuo R. 2020. Geodata Science-Based Mineral Prospectivity Mapping: A Review. *Nat Resour Res.* 29(6): 3415–3424.
- Zuo R, Agterberg FP, Cheng Q, Yao L. 2009. Fractal characterization of the spatial distribution of geological point processes. *Int J Appl Earth Obser Geoinf.* 11(6):394–402.
- Zuo R, Xia Q, Wang H. 2013. Compositional data analysis in the study of integrated geochemical anomalies associated with mineralization. *Appl Geochem.* 28:202–211.